Int. J. Solids Structures Vol. 25, No. 3, pp. 213–233, 1989
Printed in Great Britain.

0020–7683/89 $3.00 + .00

FROM THE RECTANGULAR HOLE TO THE IDEAL CRACK

P. S. THEOCARIS and L. PETROU
Department of Engineering Sciences, The National Technical University of Athens, P.O. Box 77230, Athens (GR 175-10), Greece

(*Received* 16 *May* 1987; *in revised form* 11 *February* 1988)

Abstract—The problem of a rectangular hole in an infinite elastic and isotropic plate, submitted to tension at infinity, is solved for any side ratio of the hole. It is assumed that the rectangular hole has rounded-off corners, the radii of curvature of which remain many times smaller than the short sides of the rectangles. The Muskhelishvili complex stress function $\varphi(z)$, sufficient to determine the first stress invariant needed for the solution is determined in a closed form by applying the conformal mapping method of the outside of a rectangle to the inside of a unit circle. The stress and strain distributions along the boundary of the hole, as well as inside a limited region in front of the short sides of the rectangle are accurately determined. It is proved that the method of reflected caustics is sensitive in examining the singular fields developed at the corners of the rectangles. Moreover, the minimum radii of the initial curves of the caustics are determined, outside of which the stress fields could be described by the singular solution. Experiments with reflected caustics in plexiglas plates corroborated the theoretical results.

INTRODUCTION

Searching in the abundant literature related to the experimental evaluation of the stress intensity factors at the tips of cracks and other kinds of singularities, based on the concept of LEFM, one may realize that a great deal of these experiments were executed in artificial cracks, where the crack is modelled by a rectilinear slit sawn in the plate, and the only precaution taken was that the flanks of the slit were not far away from each other. Then the stationary crack was modelled as an orthogonal narrow slit (Theocaris, 1986a).

The main difference between an actual crack and an artificial one is that in a real crack the flanks of the crack are only separated from each other by some kind of failure mechanism (cleavage, slip deformation, etc.) and no material is missing between the flanks, so that if the crack is submitted to a simple compression loading (without shear) the flanks close and there is no stress concentration appearing at the crack tip. On the contrary, in an artificial crack material is removed between the flanks of the slit and therefore the artificial crack under compression presents stress concentrations at the tip, as well as along its flanks.

Early work on the influence of the blunt tips of a crack on the stress distribution at the vicinity of the tip was carried out by Creager and Paris (1967). It was shown, among others, that the stress distribution near the singular tip for blunt cracks is the same as the stress field around a sharp crack, corrected by additional terms depending on the radius of curvature of the blunt notch. It is interesting to note that the correction terms for the normal stresses in a plane-stress problem are equal and of opposite sign, so that the first stress invariant remains always independent from these correction terms.

Thus, while the continuum model of a crack is a planar conglomeration of voids of zero thickness and the corresponding mathematical model is a plane of discontinuity, the representation of a real crack by a slit creates a third model, where the crack is represented by a removal of a rather thick layer of material. These differences in the models are striking and they are the main cause of large discrepancies in the results.

Another consequence of the difference between the models of a real and an artificial crack concerns the singularities at the crack tips and their orders. Whereas, for a real crack in an infinite elastic and isotropic plate, the order of singularity at the tip is $\lambda = 1/2$, in the artificial crack we have a pair of corners for each tip, which for simplicity may be assumed as 90°. Corners create a doublet of singularities for either corner, which, according to the theory of multiwedges, are of an order depending on the angle $(2\pi - \varphi) = 3\pi/2$ and the

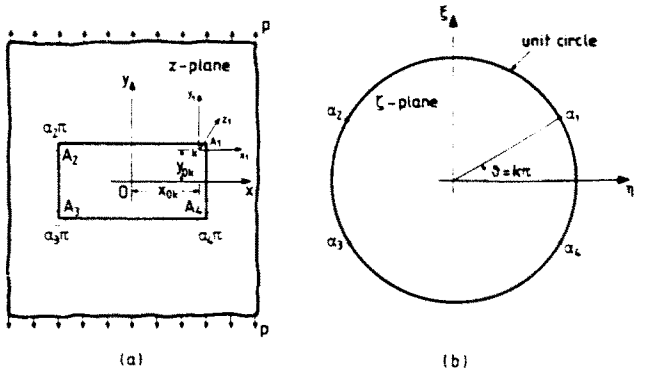

Fig. 1. (a) A plate containing a rectangular hole of a certain side ratio $m = a/b$ and an $0xy$-frame the origin of which is placed at the centre of the rectangle. (b) The transformed ζ-plane which maps the perforated plate into the interior of the unit circle.

material properties of the plate (Theocaris, 1974). This difference in the arrangement of singularities at the tips is of primordial interest.

Another interesting paper concerned with the stress field near blunt cracks and its influence on the fracture criterion of the material was presented by Kuang (1982). In this paper the two-term solution for the near-tip stress field was extended to contain the influence of the bluntness of the crack. The influence of the crack-tip radius was also studied on the fracture criterion, based on the classical S-criterion for sharp cracks. Again, in this paper, the differences in the sharp crack and the blunt crack models are considered and their influence on the form and the magnitude of the near-tip stress fields indicated.

Blunting of the cracks was also extensively considered when plastic deformation begins to be installed at the vicinity of the crack tip, when the blunting of the crack becomes conspicuous and its influence on the interaction between the crack tip and the cloud of voids developed in the vicinity of the crack tip was encountered for studying fracture processes by void nucleation, coalescence and interaction with the main crack (Theocaris, 1986b).

In this paper, the differences in the topography of the deformed elastic field around the corners of a rectangular hole in a plate submitted to tension and the deformed area at the vicinity of a mathematical model of a crack under simple tension were studied (Theocaris and Pazis, 1983).

By using the method of reflected caustics, it may be observed that, for low levels of loading, individual caustics were formed at each corner of the hole. As the loading increases the two caustics of either corner of the rectangle interact and make the caustics interfere and coalesce. As the load is further increased, a third mode of deformation may be attained, where unique caustics are formed from either pair of singularities at the corners of the rectangle. These caustics are similar to the caustics derived from the mathematical model of the crack.

The stress field around the rectangular hole was given by Savin (1961) for rounded-off corners and different side ratios. Savin's solution used the Schwarz–Christoffel transformation to map the outside of the rectangular hole to the inside of the unit circle. The transformed stress function, represented in a series expansion, was truncated to a certain number of terms, thus rounding the corners of the rectangle. In this paper the Muskhelishvili stress function, used for the solution, was expanded to an infinite number of terms, in order to assure an acceptable curvature of the corners. Moreover, the side ratio was considered as a variable, in order to form different artificial cracks with the appropriate side ratios.

THE CONFORMAL MAPPING FUNCTION

Let the z-plane in Fig. 1 represent the plate containing a rectangular hole, the side ratio $b/a = m$, and the origin of the $0xy$-frame of which is placed at the centre of the

rectangle. On the other hand, the ζ-plane represents the transform plane, where the perforated plate is mapped into the interior of the unit circle ($\rho = 1$). In the case of rectangular holes in the plate with different side ratios approximate values for the conformal mapping function $z = \omega(\zeta)$ can be readily obtained from the Schwarz–Christoffel integral given by Smirnov (1933)

$$z = \omega(\zeta) = \int_1^{\zeta} \left(1 - \frac{a_1}{t}\right)^{\alpha_1 - 1} \left(1 - \frac{a_2}{t}\right)^{\alpha_2 - 1} \left(1 - \frac{a_3}{t}\right)^{\alpha_3 - 1} \left(1 - \frac{a_4}{t}\right)^{\alpha_4 - 1} dt. \tag{1}$$

Points a_1, a_2, a_3 and a_4 on the unit circle correspond to apices A_1, A_2, A_3 and A_4 of the rectangle and they have been conveniently selected, by defining the angle $\theta = k\pi$ to satisfy the obligation to yield the given side ratio for the rectangular hole. Then, it is valid that (Savin, 1961)

$$a_1 = e^{k\pi i}, \quad a_2 = e^{(2-k)\pi i}, \quad a_3 = e^{(1+k)\pi i} \quad \text{and} \quad a_4 = e^{(1-k)\pi i}. \tag{2}$$

On the other hand, the real positive constants α_i ($i = 1, 4$) indicating the fraction of π corresponding to the exterior angles of the rectangle take the values

$$\alpha_1 = \alpha_2 = \alpha_3 = \alpha_4 = 3/2. \tag{3}$$

Then, eqn (1) may be written as

$$\omega(\zeta) = R \int_1^{\zeta} \left(1 - \frac{e^{2ik\pi}}{t^2}\right)^{1/2} \left(1 - \frac{e^{-2ik\pi}}{t^2}\right)^{1/2} dt \tag{4}$$

with $|t| \leqslant 1$.

Equation (4) may be also written as

$$\omega(\zeta) = R\left\{\frac{1}{\zeta} - \sum_{n=1}^{\infty} \beta_n \cos(2nk\pi)\zeta^{2n-1} - \frac{1}{2}\sum_{n=1}^{\infty}\sum_{j=1}^{\infty} \beta_n \beta_j \cos(2(n-j)k\pi)\right\}\zeta^{2(n+j)-1} \tag{5}$$

where coefficients β_n are given by

$$\beta_n = \frac{(-1)^n(\frac{1}{2}-0)(\frac{1}{2}-1)(\frac{1}{2}-2)\ldots(\frac{1}{2}-(n-1))}{n!}. \tag{6}$$

Finally, the $\omega(\zeta)$-function may be approximated as

$$\omega(\zeta) = R_N\left\{\frac{1}{\zeta} - \sum_{n=1}^{N} c_n \zeta^{2n-1}\right\} \tag{7}$$

where the factor R_N is a real factor characterizing the magnitude of the rectangle.

Equation (7) maps the rectangle with sharp corners to the unit circle if $N \to \infty$. If a finite number N_f is considered in the series expansion of eqn (7), the corners of the rectangle become rounded-off. They present a radius of curvature ρ_c depending on N given by

$$\rho_{cN} = \frac{(x'^2 + y'^2)^{3/2}}{|x'y'' - x''y'|} \tag{8}$$

where x, y are the coordinates of each corner of the rectangle in the complex plane $z = (x + iy)$, and they are expressed by

Table 1. The values of the constant R_N and the radii of curvature ρ_{cN}, normalized to the small side b of the rectangular hole with $m = 5.3$, 16.8, and 39.8, as well as the maximum values of the SIFs along the boundaries of the holes

$k = 5/36$		$a/b \simeq 5.23$		$k = 3/36$		$a/b \simeq 16.8$		$k = 2/36$		$a/b \simeq 39.8$	
N	R_N/b	ρ_{cN}/b	SCF_N	N	R_N/b	ρ_{cN}/b	SCF_N	N	R_N/b	ρ_{cN}/b	SCF_N
4	1.7485	0.06484	7.0530	4	4.9173	0.21812	8.2176	4	11.1931	0.59990	7.4531
5	1.7520	0.06456	7.1280	5	4.6105	0.10381	11.3227	5	10.0963	0.32863	10.0708
6	1.7278	0.04499	8.6666	6	4.7545	0.07214	13.2570	6	10.8237	0.21431	13.0865
7	1.7470	0.02900	10.5610	7	4.7050	0.06606	13.4336	7	10.3228	0.12829	16.3772
8	1.7406	0.02651	10.7750	8	4.6981	0.06559	13.5263	8	10.6389	0.09113	19.3401
9	1.7368	0.02513	11.1924	9	4.7321	0.05870	14.5311	9	10.4508	0.07180	21.1086
10	1.7441	0.01900	12.8520	10	4.6913	0.04552	16.4742	10	10.5420	0.06713	21.5540
11	1.7390	0.01534	14.0033	11	4.7265	0.03441	18.7931	11	10.5177	0.06663	21.4862
12	1.7397	0.01527	13.9842	12	4.7029	0.02826	20.3381	12	10.4974	0.06577	21.7034
13	1.7422	0.01377	14.8214	13	4.7133	0.02698	20.6268	13	10.5441	0.06201	22.5591
14	1.7391	0.01100	16.4067	14	4.7142	0.02696	20.6548	14	10.4852	0.05430	24.1158
15	1.7407	0.01015	16.8970	15	4.7058	0.02531	21.3973	15	10.5459	0.04590	26.2739
16	1.7412	0.01007	17.0071	16	4.7175	0.02186	23.0322	16	10.4909	0.03765	28.7350

$$x = R_N\left\{\cos\theta + \sum_{n=1}^{N} c_n \cos[(2n-1)\theta]\right\} \tag{9}$$

$$y = R_N\left\{-\sin\theta + \sum_{n=1}^{N} c_n \sin[(2n-1)\theta]\right\}. \tag{10}$$

Here the primes and double primes denote differentiation with respect to the angle θ for values of $\theta = k\pi$.

If it is desired that all the rectangles for different values of N maintain the same small side b, the real constant R_N may take the values

$$R_N = \frac{b}{2}\frac{1}{1+\sum_{n=1}^{n}(-1)^n c_n}. \tag{11}$$

The values of constant R_N and of the radii of curvature ρ_{cN} normalized to the small side, b, of the rectangle are given in Table 1 for parametric values of k and therefore of the side ratio a/b.

Three different rectangles were examined with side ratios $\lambda = 5.23$, 16.8 and 39.7 with $k = 5/36$, 3/36 and 2/36. It may be observed that the greater the number of terms, N, in eqn (7) the smaller are the values of the radii of curvature of the corners of the rectangles $\rho_c N/b$, normalized to the side b, whereas the ratio R_N/b remains almost constant.

Since the finest cutter for sawing an artificial slit could have a thickness of the order of $d = 0.0003$ m, then the lengths of the crack for the above examined three cases are respectively $a = 0.0016$, 0.005 and 0.015 m, which, especially the third one, are suitable for initial cracks in the fracture mechanics tests. On the other hand, the radii of curvature at the corners take values varying between $\rho_{cN}/b = 0.3$ and 0.03.

EVALUATION OF THE STRESS CONCENTRATION FACTORS AT THE CORNERS

For an infinite plate submitted to a tensile stress, p, at infinity, parallel to the Oy-axis, passing through the origin O lying at the centre of the rectangular hole, the complex potential function $\varphi(z)$ is given by (Muskhelishvili, 1953)

$$\varphi(z) = \frac{pz}{4} + \varphi^*(z). \tag{12}$$

The function $\varphi(z)$ in the mapped ζ-plane is expressed by

$$\varphi(\zeta) = \frac{p}{4}[\omega(\zeta)] + \varphi_0(\zeta) \tag{13}$$

where $\varphi_0(\zeta)$ is a function expressed by

$$\varphi_0(\zeta) = \sum_{r=1}^{\infty} \varepsilon_r \zeta^r = \sum_{r=1}^{\infty} \{\text{Re } \varepsilon_r + \text{i Im } \varepsilon_r\}\zeta^r \tag{14}$$

where ε_r's are complex constants.

The boundary conditions for the basic stress field are given by

$$f_1^0 + \text{i} f_2^0 = -\frac{p}{2}[\omega(\sigma) - \text{e}^{2\text{i}\alpha}\overline{\omega(\sigma)}] \tag{15}$$

where exponent α denotes the angle subtended by the external loading axis and the Ox-axis of the rectangle, and σ represents the points along the boundaries of the hole and of the circumference of the unit circle in the mapped plane ζ.

For the determination of the unknown φ_0-function use was made of the integral equation given by Savin (1961)

$$\varphi_0(\zeta) + \frac{1}{2\pi\text{i}} \int_\gamma \frac{\omega(\sigma)}{\overline{\omega'(\sigma)}} \overline{\varphi_0'(\sigma)} \frac{\text{d}\sigma}{(\sigma - \zeta)} = \frac{1}{2\pi\text{i}} \int \frac{f_1^0 + \text{i} f_2^0}{(\sigma - \zeta)} \text{d}\zeta \tag{16}$$

where now ζ is a point inside the unit circle γ. The integral on the left-hand side of eqn (16) may be approximated to

$$\varphi_0(\zeta) + \frac{1}{2\pi\text{i}} \int \frac{\omega(\sigma)}{\overline{\omega'(\sigma)}} \overline{\varphi_0'(\sigma)} \frac{\text{d}\sigma}{(\sigma - \zeta)} = \sum_{n=1}^{N} \sum_{r=1}^{2(N-n)} rP(n)(\text{Re } \varepsilon_r - \text{i Im } \varepsilon_r)\zeta^{N-n-2} + \sum_{r=1}^{\infty} (\text{Re } \varepsilon_r + \text{i Im } \varepsilon_r)\zeta^r \tag{17}$$

where the $P(n)$ are given by the recurrence formula

$$P(n) = c_{N-n+1} - P(1)c_{n-1}[2(n-1)-1] - \cdots - P(n-1)c_1$$

with $P(1) = -c_N$.

On the other hand, the integral on the right-hand side of eqn (16) is approximately expressed by

$$\frac{1}{2\pi\text{i}} \int_\gamma \frac{f_1^0 + \text{i} f_2^0}{(\sigma - \zeta)} \text{d}\sigma = -\frac{pR_N}{2} \left\{ \sum_{n=1}^{N} c_n \zeta^{(2n-1)} - \text{e}^{2\text{i}\alpha}\zeta \right\}. \tag{18}$$

Comparing now the coefficients of the corresponding real and imaginary parts in the respective terms of power of ζ in eqns (17) and (18), we obtain a system of $2(2N-1)$ equations which when solved yields the values of the real and imaginary parts of ε_r.

If relations (7) and (14) are introduced into relation (13) they yield the following expression for the $\varphi_n(\zeta)$-function:

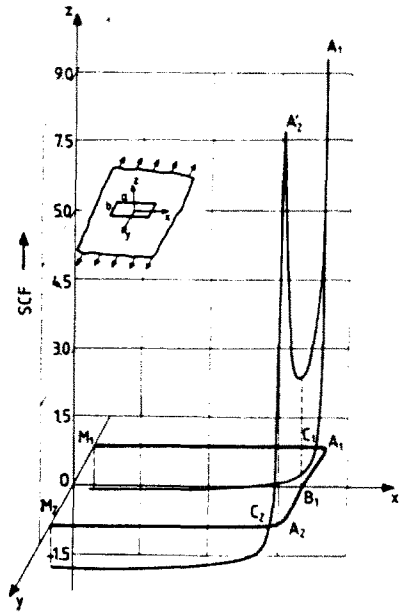

Fig. 2. The distribution of the stress concentration factor along the boundaries of the rectangular hole in a plate submitted to simple tension at infinity.

$$\varphi_n(\zeta) = \frac{pR_N}{4}\left\{1 + \sum_{n=1}^{N} c_n\zeta^{2n-1}\right\} + \sum_{r=1}^{2N-1} \varepsilon_r\zeta^r. \tag{19}$$

Since along the boundary of the rectangular hole the normal to the boundary component of the normal stresses is zero, it remains from the first stress invariant only the σ_φ-component, parallel to the boundary of the hole. Then, it is valid that (Smirnov, 1933)

$$\sigma_\varphi = 4\ \mathrm{Re}\left[\frac{\varphi'(\zeta)}{\omega'(\zeta)}\right]. \tag{20}$$

This value for σ_φ becomes equal to infinity for $\omega'(\zeta) = 0$, that is, at the sharp corners of the rectangular holes. For rounded-off apices of the hole the σ_φ-stress becomes a maximum without tending to infinity. This maximum value, normalized to the applied tensile stress at infinity, p, yields the stress concentration factor at the respective corner. The SCF is given by

$$\mathrm{SCF}_N = 4\ \mathrm{Re}\left[\frac{\varphi'_N(e^{ik\pi})}{\omega'_N(e^{ik\pi})}\right]. \tag{21}$$

Figure 2 presents the distribution of the stress concentration factors along the boundaries of the rectangular hole in a plate submitted to simple tension at infinity, normal to the long side of the rectangle. The rectangular hole corresponds to $k = 5/36$ and it was taken as $N = 4$. It may be observed from the SCF-distribution that the small side, b, of the rectangle is under tension with maximum stress concentrations at corners A_1 and A_2, as expected, and minima at the mid-length B_1 of the short side A_1A_2 of the rectangle. On the contrary, the SCFs along the long side diminish rapidly from their values $A_1A'_1$ and $A_2A'_2$ at the corners, they pass through zero at points C_1 and C_2, and they become negative indicating a compressive state of stress along the long sides. Again, the minimum compressive SCF appears at the middle points M_1 and M_2 of the long sides, but this minimum is smooth, since along the greater part of the long side the SCF varies only very little.

It is worthwhile to evaluate the u_z-displacement along the thickness of the plate. For plane-stress conditions in the plate the u_z-displacement is given by

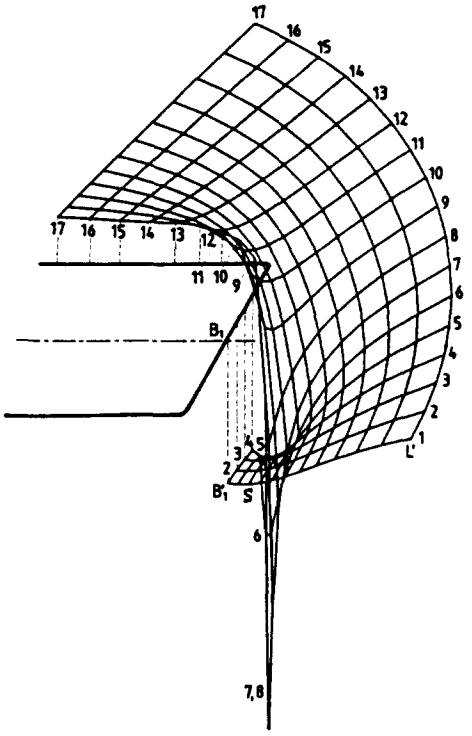

Fig. 3. The shape of the deformed lateral upper face of the plate at the vicinity of the short side of the rectangular artificial crack, as plotted by computer.

$$u_z = -\frac{2\nu d}{E}\,\mathrm{Re}\,\frac{\varphi'_N(\zeta)}{\omega'_N(\zeta)} \tag{22}$$

where d is the thickness of the plate, ν and E are Poisson's ratio and the elastic modulus of the material of the plate and Re indicates the real part of the ratio of functions $\varphi'_N(\zeta)$ and $\omega'_N(\zeta)$ in the ζ-plane.

In Figs 2 and 3 the quantities plotted by computer were presented in an axonometric projection, in order to show the variation of these quantities in space along the boundaries of the rectangular crack, which is inclined to a 60°-projection.

Figure 3 presents the shape of the deformed surface of the upper face of the plate at the vicinity of the short side of the rectangular crack, as plotted by computer. Corners A_1 and A_2 present very abrupt craters, due to the singular stresses there. The depths $A_1A'_1$ and $A_2A'_2$ corresponding to the craters at the corners represent the maximum submersions of the lateral faces of the plate. On the other hand, the submerged middle point B_1 of the short side of the rectangle goes to B'_1, which corresponds to the point of minimum submersion of the boundaries of the rectangular crack.

The deformed lateral face of the plate then takes the form of a saddle at the vicinity of the short side of the rectangular crack. The lateral deformed Ox-axis between points B_1 and L_1 goes to the $B'_1L'_1$-curve, which presents a relative minimum inside the plate at point S, which really corresponds to the bottom of the ridge of the saddle-like surface of the plate at the vicinity of the rectangular crack.

THE REFLECTED CAUSTICS FROM THE CORNERS OF THE RECTANGULAR CRACK

It has been shown (Theocaris, 1981) that for an elastic plane-stress field only the one Muskhelishvili complex potential, $\phi(z)$, suffices to express the generatrix curve of the caustic, formed when the rays of a light beam are reflected from the close vicinity of the singular zones of the stress field. This curve is given by

$$|C\phi''(z)| = 1. \tag{23}$$

This generatrix curve, called the *initial curve*, forms in space a caustic surface, the intersection of which with a reference plane, placed at a distance z_0 from the stress field, is a caustic curve expressed by

$$W = \lambda_m(z + C\overline{\phi'(z)}). \tag{24}$$

In these relations C is an overall constant containing the mechanical and optical properties of the plate and the characteristic dimensions of the optical arrangement and λ_m is the magnification factor of the optical set-up, given by

$$\lambda_m = \frac{z_0 + z_i}{z_i} \tag{25}$$

where z_i is the distance between the focus of the light source and the specimen.

The function $\phi(z)$, the first and second derivatives of which enter into the expressions for the caustic and its initial curve, is given by

$$\phi(\zeta) = \frac{\varphi'(\zeta)}{\omega'(\zeta)}.$$

Then, these derivatives are expressed by

$$\phi'(z) = \frac{\phi'(\zeta)}{\omega'(\zeta)}$$

$$\phi''(z) = \frac{1}{[\omega'(\zeta)]^2}\left\{\phi''(\zeta) - \phi'(\zeta)\frac{\omega''(\zeta)}{\omega'(\zeta)}\right\}. \tag{26}$$

In these relations $\phi'(\zeta)$ and $\phi''(\zeta)$ are the first and second derivatives of the complex potential $\phi(\zeta)$.

The constant C is expressed by

$$C = \frac{4z_0 dc_{r,f}}{\lambda_m} \tag{27}$$

where the only unknown is the optical constant for the material of the plate, which for reflections from the rear face (c_r) must be measured by interferometry, whereas for reflections from the front face takes the value $c_f = \nu/E$. Finally, z is the complex distance in the plane of the plate ($z = x + iy$) and W expresses the vector of deviation of the light rays on the plane of reference, where the caustic is formed.

Relation $\phi''(z)$ in eqns (26) may be written in the form

$$\phi''(z) = \frac{p}{R_N^2} f(\zeta) \tag{28}$$

where $f(\zeta)$ is a polynomial function of ζ, which does not present singular points. This is due to the fact that the $\omega'(\zeta)$-function is different than zero all over the plate since the orthogonal hole has rounded-off corners in this plane. The constant coefficients of the polynomial depend on the ratio m of the sides of the hole and the desired curvature at its apices.

The $\phi''(z)$-function is also proportional to the applied stress p at infinity of the plate and inversely proportional to the square of the major axis of the hole, which is expressed by the quantity R_N.

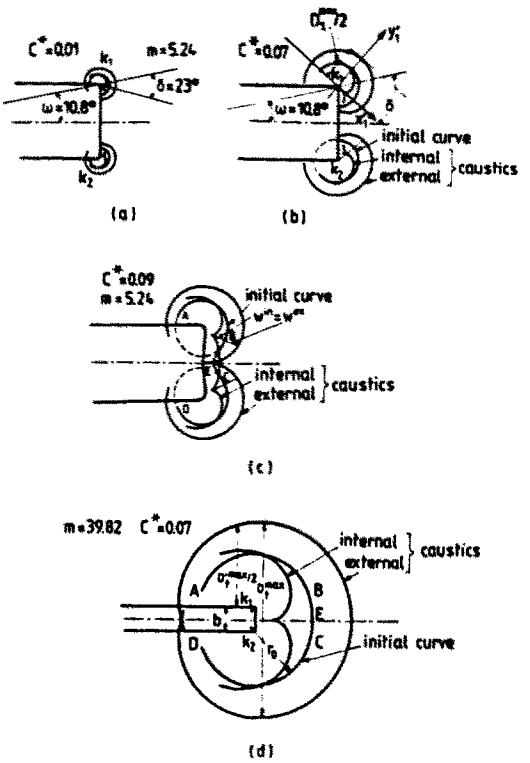

Fig. 4. The initial curves and the caustics of an infinite thin plate containing rectangular internal holes with rounded-off corners for $m = 5.3$ having radii of curvatures $\rho_{c10} = 0.019b$ ((a) and (b)) and $\rho_{c4} = 0.06b$ (c), while (d) corresponds to a hole with $m = 39.8$ and with respective radii $\rho_{c10} = 0.067b$.

The equation for the initial curve (eqn (23)) may be written as

$$|C^* f(\xi)| = 1 \tag{29}$$

where

$$C^* = C\frac{p}{R_N^2}.$$

The overall constant C^* is a non-dimensional quantity and it contains the characteristic quantities of the optical setup z_0 and λ_m, the stress optic coefficient c_r, the thickness d of the plate which must assure plane-stress conditions, the applied stress p at infinity and the ratio m.

The solution of eqns (29) and (24) is achieved numerically by a convenient computer program. Figure 4 presents the initial curves and the reflected caustics of an infinite thin plate containing rectangular internal holes with rounded-off corners for $m = 5.3$, having radii of curvature $\rho_{c10} = 0.019b$ (Fig. 4(a)), as well as for $m = 39.8$ and respective radii $\rho_{c10} = 0.067b$ (Fig. 4(d)). The index 10 in the radii of curvature means that these radii correspond to values derived from 10 terms in the series approximations of the $\phi(z)$-function.

Figure 4(b) for $C^* = 0.07$ yields initial curves separated from each other for each corner of the hole. This means in such radii the craters at each corner are independent of each other and in these radii of initial curves the u_z-displacement contour lines are independent of each other. Moreover, the initial curves for these corners may be approximated to a high degree of accuracy as circles with centres the points k_1 and k_2 coinciding with the virtual singular points of the plate (Theocaris and Petrou, 1986).

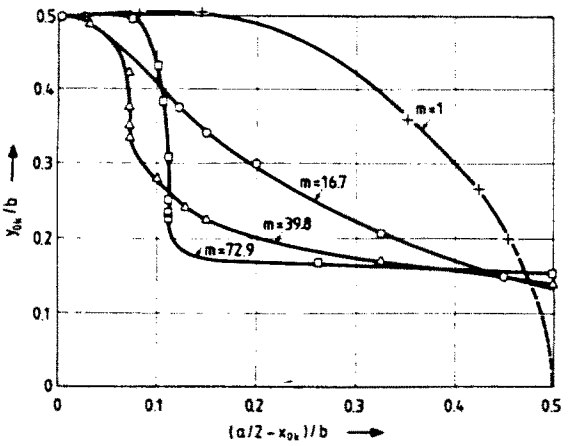

Fig. 5. The evolution of the position of the centre k_1 of one circular branch (AB) of the initial curve for rectangular holes with side ratios m = 1.0, 11.8, 39.8 and 72.9, respectively.

The internal caustics at each corner present cusps derived from the reflections of light rays from the local minimum points of the u_z-displacement craters along each initial curve. The vector W defining the caustic is normal to the tangent of the initial curve at these local minima, whereas for the external branches of caustics these points yield local maxima in the respective caustics.

For increasing values of C^* attaining a value $C^* = 0.09$, which is achieved by changing the arrangement of the optical set-up without changing the loading conditions of the plate, the initial curves at the respective corners of the minor side of the rectangle evolute to a unified curve shown in Fig. 4(c). This curve is formed from segments AB and CD which are to a good approximation parts of circumferences with centres k_1 and k_2, connected by the adaptation curve BEC. The AB and CD circular segments lie inside either crater whereas the BEC segment traverses the hill formed between the two craters of the corners.

Moreover, the caustics for $C^* = 0.09$ also are unified, presenting an internal caustic with two cusp points and the external caustic with one smooth cusp zone. The cusp points of the internal caustic are derived from points B and C of the initial curves lying inside the craters of the u_z-displacements of either corner, whereas the cusp zone of the external caustic originates at point E of the intersection of the transverse axis of the hole and the initial curve for the rear face, the point which corresponds to a local minimum.

The vector $W_E^{int} = W_E^{ex} = 0$ when the initial curves pass through point S of the longitudinal axis of the rectangular hole (Fig. 3). When point E lies on the $B_1'S$ segment then the internal and the external caustics cross each other, whereas when point E lies on the SL segment the respective caustic lie on both sides of the initial curve, separated from each other.

For values of C^* higher than the above value the initial curves envelop both craters without penetrating in either of them. Figure 4(d) shows such a case of initial curves formed in a rectangular hole having a side ratio $m = a/b = 39.8$ and an overall constant C^* taking the value 0.07. In this case also each initial curve is formed, to a good approximation, by the circular segments AB and CD with centres k_1 and k_2, respectively, joined together by the adaptation curve BEC. In this case, however, only the internal caustic presents a unique cusp point, which is generated by point E of the initial curve. This point is a local minimum of the u_z-displacements when this curve lies outside both craters of the corners (Fig. 3). This caustic resembles the caustic corresponding to a mathematical crack disposing a single crater.

Figure 5 shows the evolution of the positions of the centre k_1 of the one circular sector AB of the initial curve for rectangular holes with side ratios m = 1.0, 16.7, 39.8 and 72.9. One may observe in this figure that these centres, when the respective initial curves lie inside the crack craters, have an almost stationary position near the rounded-off corners of the hole. When the initial curves are partly getting out of the craters, these centres move towards the centre of symmetry of the hole.

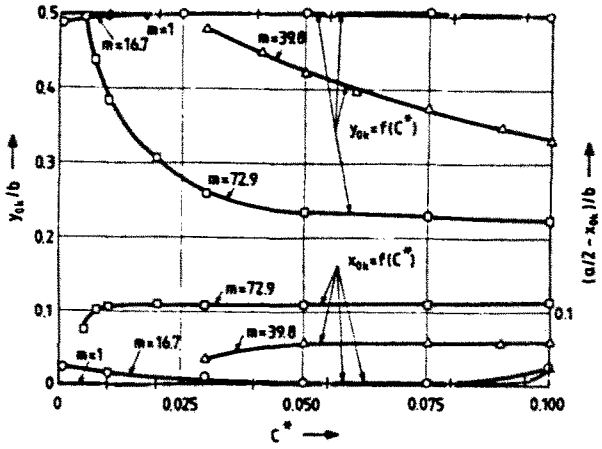

Fig. 6. The values of the y_{0k}- and x_{0k}-coordinates of the centres k_i of the initial curves, vs the values of overall constant C^*, lying inside the interval $0 < C^* \leqslant 0.1$.

For the case of a square hole with $m = 1.0$ point k_i is stationary for $C^* \leqslant 1.0$ and then follows a parabolic path tending towards the centre of the square. In this case the respective centres k_i are equally attracted from all corners of the square and they tend symmetrically to the centre of the hole.

For $m = 39.8$, for a curvature radius of the rounded-off corners equal to $\rho_{c10} = 0.067b$ and for values of $C^* < 0.03$ the centres of the initial curves remain stationary. For values of $C^* > 0.03$ these centres move rapidly, almost normally, at a distance equal to $0.1b$ from the minor side of the hole and then move toward the centre of the rectangle. A similar movement presents the points k_i for the hole with $m = 72.9$, whereas for $m = 11.8$ points k_i follow an almost straight line inclined to 45° to the sides of the rectangular hole for values of $C^* > 0.3$.

In Fig. 6 the values of the y_{0k} and x_{0k} coordinates of the centres k_i are presented vs the values of the overall constant C^* lying inside the interval $0 \leqslant C^* \leqslant 0.1$. This interval is the most important, because for such ratios of m and loading steps C^*, the rectangular holes assimilating artificial cracks are normally tested in the experiments.

THE COMPLEX POTENTIAL FUNCTION $\phi(z) = K/2(2z)^{\lambda}$

Let us assume a stress field which is described by the complex potential (Theocaris, 1975)

$$\phi(z) = \frac{K}{2(2z)^{\lambda}} \tag{30}$$

where K represents the complex SIF and λ is the respective order of singularity in this field. The initial curve of this field is given from relation (23) and it is expressed by

$$|\lambda(\lambda+1)C|K||/|2^{(\lambda+1)}(z)^{\lambda+2}| = 1. \tag{31}$$

We may observe that the initial curve is a circle of radius r_0 given by (Theocaris and Prassianakis, 1980)

$$r_0 = \left|\frac{\lambda(\lambda+1)}{2^{(\lambda+1)}} C|K|\right|^{1/(\lambda+2)} \tag{32}$$

with its centre lying at the point $z = 0$.

The respective caustic is given in parametric form as follows [10]:

$$X = \lambda_m r_0 \left[\cos \varphi + \frac{\varepsilon}{(\lambda+1)} \cos (\varphi(1+\lambda) - \omega) \right]$$

$$Y = \lambda_m r_0 \left[\sin \varphi + \frac{\varepsilon}{(\lambda+1)} \sin (\varphi(1+\lambda) - \omega) \right]. \tag{33}$$

The quantities r_0 and φ express in polar coordinates the points of the initial curves and ε is given by $\varepsilon = \text{sign } c/|c|$ taking the value $\varepsilon = 1$ for reflections from the rear face and $\varepsilon = -1$ for reflections from the front face of the cracked plate. Angle ω is expressed by

$$\omega = \tan^{-1} (\mu) = \tan^{-1} \left(\frac{K_{II}}{K_I} \right) \tag{34}$$

or

$$K = (K_I - iK_{II}) = |K| \exp (-i\omega).$$

By rotating the reference frame, $k_1x_1y_1$ in Fig. 4(b), by an angle $\delta = \omega/\lambda$ in the new position $k_1x'y'$, as it has been done by Williams (1957), the parametric equations of the caustics are simplified as follows:

$$X' = \lambda_m r_0 \left[\cos \varphi' + \frac{\varepsilon}{(1+\lambda)} \cos (1+\lambda)\varphi' \right]$$

$$Y' = \lambda_m r_0 \left[\sin \varphi' + \frac{\varepsilon}{(1+\lambda)} \sin (1+\lambda)\varphi' \right]. \tag{35}$$

Equations (35) represent the caustic of Fig. 4(b) which is referred to the frame $k_1x'y'$ with an axis of symmetry the k_1x'-axis. The maximum transverse diameter of this caustic $D_t^{max} = 2Y'_{max}$ is parallel to the k_1y'-axis and it is given by (Theocaris and Petrou, 1987)

$$D_t^{max} = 2\lambda_m r_0 \left[\sin \frac{\pi}{(2+\lambda)} + \frac{1}{(1+\lambda)} \sin \frac{\pi(1+\lambda)}{(2+\lambda)} \right]. \tag{36}$$

Furthermore, in the $k_1x'y'$ system of axes it is valid that $|K| = |K_I^*|$ and therefore

$$K_I^* = r_0^{(2+\lambda)} \frac{2^{(1+\lambda)}}{\lambda(1+\lambda)C}. \tag{37}$$

By studying the caustics formed by initial curves lying inside the craters of each rounded-off corner of the rectangular hole we observe that the angle, δ (see Fig. 4(a), (b)), of rotation of the caustic remains almost constant for radii of the initial curves satisfying the condition $r_0 \leqslant 0.12b$. For values $r_0 > 0.12b$ the angle of rotation of the caustic increases rapidly in the area of values of r_0 tending to yield a unified caustic, enveloping the minor side of the rectangle. Subsequently the two cusps of the internal caustic approach each other and they are displaced in the interior of the hole, whereas the unique cusp of the external caustic recedes from the hole.

For values $r_0 > 1.20b$ the two cusps of the internal caustic coalesce, whereas the cusp of the external caustic disappears. The final form of the caustics for high values of C^* and therefore for increased steps of the loading of the plate is presented in Fig. 4(d) and resembles the caustics of Griffith cracks.

Therefore, according to the previously established evidence, the evaluation of SIF and of the SO according to the theory developed in this paper, may be carried out with accuracy only in the regions where $r_0 \leqslant 0.12b$ or $r_0 \geqslant 1.20b$.

Indeed, in the region where $r_0 < 0.12b$ it may be evaluated from the angle δ of rotation of the caustic as well as from the ratio of the diameter of the caustic and the radius of its initial curve that the order of singularity tends to the value $\lambda = 0.455$, which is given by Williams (1957) for a notch of an angle $\varphi = \pi/2$.

The SO for the caustic of Fig. 4(a) is evaluated (Theocaris, 1975) as $\lambda \simeq 0.47$. The determination of K_I and K_{II} may then be readily carried out by using relations (37) and (34). The region of validity of these values is rather small and without practical meaning for artificial cracks of the experiments. On the contrary, great interest presents the region $r_0 > 1.20b$ for the evaluation of K_I, since in this region an overall SIF may be evaluated from the unified caustic, which is a mode-I SIF since the rotation of the caustic is annuled.

Tables 2–4 contain the values of SIFs and SOs describing the stress field around the centre k_i of the initial curves. This region is extended to the longitudinal axis of symmetry of the cracked plate, whereas the other half is symmetric to this one. In the same tables the coordinates of the centres k_i of the initial curves in columns 3 and 4 (see also Fig. 1) are given, as well as the values of λ and K_I/p in columns 10 and 11.

The values of K_I as they have been derived from the diameter D_i^{max} of the caustic assuming as $\lambda = 1/2$ are given in column 12, whereas the discrepancies between these values and the theoretical ones based on the relation $K_I = \sigma_\infty \sqrt{a}$ for a natural crack are included in column 13.

While Table 2 contains the case of a rectangular hole with $m = 39.8$, Table 3 corresponds to $m = 72.9$ and Table 4 to the Griffith crack. The selected values of m's are those which are frequently met in artificial cracks of experiments.

Figure 7 gives the values of the radii of the initial curves normalized to the half-crack length vs the overall constant C^*. One may observe that the values of r_0/a for $C^* \leqslant 0.025$ coincide with the respective values of the Griffith crack, whereas the rectangular hole with $m = 39.8$ does not present a caustic of the form of Fig. 4(c) in this region.

It is worthwhile noting that almost all of the experimental cracks, when they are artificial, lie in the zone $40 \leqslant m \leqslant 70$ and the experimental set-up, the crack length, the thickness of the specimens and the external loading are such that they yield values for K_I which differ between them only by 5%. Moreover, in the applications of caustic nobody evaluates the radius of the initial crack, but calculates directly, from the diameter of the caustic the respective value of SIF.

In order to check the stress field near the corners of the rectangular hole, as it is derived from the proposed method evaluating K_I and λ, the values of the sum of the principal stresses were checked with the values derived from the theoretical solution giving $K_I = p\sqrt{a}$ and $\lambda = 1/2$. This sum was calculated according to the two methods along the long axis of symmetry of the rectangular hole (see Fig. 10).

While the traces marked as I represent the theoretical values, traces II correspond to $K_I/p = (0.929/2)^{1/2} = 0.603^{-3/2}$, $\lambda = 0.50$ with origin the point $(x_{0k}/b = 36.35, y_{0k}/b = 0)$, and traces III to values of the sum corresponding to $K_I/p = 0.4208$ and $\lambda = 0.57$ with a centre having coordinates $x_{0k_1}/b = 36.35$ and $y_{0k_1}/b = 0.25$. It is clear from these curves that an improvement of the values of the sum of normal stresses relative to the theoretical values as defined by the method of this paper is achieved when these values are compared with the respective curves corresponding to the singular solution.

EXPERIMENTAL EVIDENCE

A series of tests was undertaken for the study of the caustics appearing at the corners of artificial cracks existing inside infinite plates submitted to simple tension at infinity. For this purpose three series of specimens made of PMMA were used. The dimensions of the specimens were: width $w = 0.10$ m, length outside the jaws $l = 0.20$ m, thickness $d = 0.003$ m. In all these specimens internal slits parallel to the short edges of the plates and at their mid points between jaws were cut with a very fine saw of thickness $t = 0.0003$ m. The ratio of the sides of the rectangular holes $m = a/b$ were taken equal to 5.3, 40 and 73, whereas the lengths of the artificial cracks were respectively 0.025, 0.012 and 0.021 m. Finally, the angles at the corners of the rectangles were rounded off with curvature radii approximately

Table 2. The values of SIFs and SOs describing the stress field around the centres k_1 of the initial curves of a rectangular hole with $m = 39.8$. The coordinates of the centres k_1 of the initial curves are given in columns 3 and 4. The values of K_1 as they have been derived from the diameter D_1^{max} of the caustic assuming $\lambda = 1/2$ (column 12), and the discrepancies between these values and the theoretical ones, based on the relation $K_1 = p\sqrt{(a/2)}$ for the natural crack (column 13)

1	2	3	4	5	6	7	8	9	10	11	12	13
a/a	C^*	x_{0k}/b	y_{0k}/b	r_0/b	$2r_0/a$	D_1^{max}/b	$D_1'^{max}\,b$	$D_1'^{max}/r_0$	λ	$\frac{K_1/p}{m^{\lambda-2}}$	$\frac{K_1/p}{m^{-3/2}}$ when $\lambda = \frac{1}{2}$	Percentage error (%)
1	0.03	19.87	0.48	1.55	0.078	5.88	4.92	3.174	0.495	0.349	0.530	16
2	0.05	19.85	0.42	2.00	0.100	7.05	6.21	3.105	0.550	0.291	0.500	11
3	0.07	19.84	0.38	2.335	0.117	7.96	7.20	3.083	0.570	0.273	0.484	8
4	0.09	19.84	0.36	2.61	0.131	8.73	8.01	3.068	0.580	0.268	0.474	6
5	0.10	19.84	0.34	2.745	0.137	9.08	8.40	3.060	0.585	0.274	0.471	5.5
6	0.20	19.82	0.28	3.70	0.186	11.72	11.16	3.016	0.620	0.244	0.446	0.0
7	0.30	19.79	0.24	4.385	0.220	13.60	13.12	2.992	0.635	0.237	0.431	−3.5
8	0.40	19.76	0.23	4.935	0.247	15.12	14.66	2.970	0.655	0.221	0.422	−6

$a/b = m = 39.83$; $R_{10} = 0.1054$ m.

Table 3. The values of SIFs and SOs describing the stress field around the centres k_1 of the initial curves of a rectangular hole with $m = 73$. The coordinates of the centres k_1 of the initial curves are given in columns 3 and 4

1	2	3	4	5	6	7	8	9	10	11	12	13
a/a	C^*	x_{0k}/b	y_{0k}/b	r_0/b	$2r_0/a$	D_1^{max}/b	$D_1'^{max}\,b$	$D_1'^{max}\,r_0$	λ	$\frac{K_1/p}{m^{\lambda-2}}$	$\frac{K_1/p}{m^{-3/2}}$ when $\lambda = \frac{1}{2}$	Percentage error (%)
1	0.005	36.38	0.49	1.32	0.036	5.26	4.28	3.242	0.45	0.586	0.753	20
2	0.0075	36.35	0.43	1.65	0.045	6.050	5.19	3.145	0.52	0.438	0.712	15
3	0.011	36.35	0.38	1.98	0.054	6.96	6.20	3.131	0.53	0.447	0.689	12
4	0.020	36.34	0.30	2.61	0.072	8.68	8.08	3.095	0.55	0.443	0.658	8
5	0.030	36.34	0.27	3.10	0.085	10.04	9.50	3.065	0.58	0.392	0.631	4.5
6	0.040	36.34	0.25	3.485	0.096	11.24	10.74	3.081	0.57	0.418	0.627	4
7	0.050	36.35	0.25	3.81	0.105	12.24	11.74	3.081	0.57	0.421	0.622	3
8	0.075	36.34	0.23	4.50	0.123	14.25	13.79	3.065	0.58	0.410	0.606	0.5
9	0.100	36.35	0.22	5.055	0.139	15.90	15.46	3.060	0.58	0.411	0.598	−0.01

$a/b = m = 72.92$; $R_{10} = 0.18853$ m.

Table 4. The values of SIFs and SOs describing the stress field around the centres k_1 of the initial curves of a Griffith crack. The coordinates of the centres k_1 of the initial curves are given in columns 3 and 4

1	2	3	4	5	6	7	8	9	10	11	12	13
a/a	C^*	$x_{0k}/(a/2)$	y_{0k}/a	r_0/b	$2r_0/a \times 10$	$D_1^{max}/a \times 10$	$D_1'^{max}/a \times 10$	$\delta = D_1'^{max}/r_0$	λ	$\frac{K_I/p}{m^{\lambda-2}}$	$\frac{K_I/p}{m^{-3/2}}$ with $\lambda = \frac{1}{2}$	Percentage error (%)
1	0.01	0.9997	—	—	0.5352	1.6794	1.6794	3.138	0.525	0.2643	3.308	2.5
2	0.03	0.9993	—	—	0.8305	2.5861	2.5861	3.113	0.542	0.2388	0.3022	4.4
3	0.05	0.9989	—	—	1.0190	3.1656	3.1656	3.106	0.547	0.2334	0.3006	4.9
4	0.07	0.9985	—	—	1.1657	3.6104	3.6104	3.097	0.554	0.2248	0.2983	5.6
5	0.09	0.9982	—	—	1.2888	3.9790	3.9790	3.087	0.562	0.2150	0.2959	6.4
6	0.10	0.9980	—	—	1.3448	4.1488	4.1488	3.085	0.564	0.2194	0.2956	6.5
7	0.50	0.9917	—	—	2.5600	7.6850	7.6850	2.002	0.630	0.1570	0.2760	12.7
8	1.00	0.9890	—	—	3.4000	9.9448	9.9448	2.920	0.693	0.1222	0.2696	14.8

$a/b = m = \infty$; $R_\infty = 0.1054$ m.

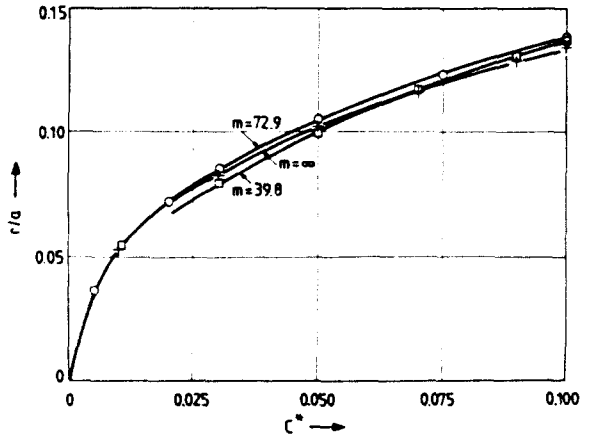

Fig. 7. The values of the radii of initial curves, normalized to the half crack length, vs the overall constant C^* for the rectangular holes with $m = 39.8$, 72.9 and ∞.

equal to $0.06b$ for each type of crack. The shapes of the cracks are given in Figs 8(a) and 9(a), respectively.

It was evaluated for such dimensions of the artificial cracks that the number of terms N should be 4, as this can be derived from Table 1. Indeed, we can achieve a very good approximation in the series expansion of $\phi(z)$ for $N = 4$ and $m = 5.3$ yielding a radius of curvature $R_4 = 0.0087$ m. For the specimens with $m = 40$ it is necessary to consider 10 terms and obtain a radius $R_{10} = 0.0032$ m, whereas for the specimens with $m = 73$ the radius R_{10} becomes $R_{10} = 0.0054$ m. We may observe that the radii R for all these cases tend to be equal to one quarter of the length of the artificial crack.

The optical arrangement for applying the method of caustics is a typical one described previously (Theocaris, 1981). The optical constants of the material used in the tests were evaluated to be $c_r = -3.34 \times 10^{-10}$ m^2 N^{-1} and $c_f = 1.0 \times 10^{-10}$ m^2 N^{-1}. Figures 8(b) and (c) present the caustics for the specimen with $m = 5.3$ for $C^* = 0.065$ (Fig. 8(b)) and 0.135 (Fig. 8(c)).

We may observe that for $C^* = 0.065$ we dispose two caustics for either corner of the artificial crack, whereas for $C^* = 0.135$ we obtain only a unified caustic for both corners of the minor side of the rectangle for reflections from the rear faces of the specimens.

This caustic presents a single cusp point. It is clear that this experimental evidence corroborates the findings of the theory concerning the shape and size of the caustics.

Figure 9(a) presents the unloaded perforated plates for $m = 40$ and 73, respectively, in a magnification corresponding to $\lambda_m = 15.0$. Figures 9(b) and (c) show the experimental and the theoretical caustics when C^* takes the values 0.2 and 0.1, respectively. Again a satisfactory coincidence appears between the theoretical and experimental caustics.

The values of D_t^{max}/a derived from the experiments and the theory present a deviation of 1.5% for $m = 40$ and 1.0% for $m = 73$. The error in the experimental evaluation of K_I depends on the error of estimating the size of the maximum transverse diameter D_t^{max} of the caustic raised to a power equal to the exponent of this diameter appearing in the respective relationship. This error was estimated to be of the order of 3% which explains the existing discrepancies between theory and experiments.

RESULTS AND DISCUSSION

Most experimenters have recourse to artificial cracks for the study of the stress fields in cracked plates instead of natural cracks. This is done because the preparation of a natural rectilinear crack is difficult to achieve satisfactorily, especially when a particular orientation of the crack axis is obligatory. However, the artificial crack is always a rectangular hole with a defined ratio $m = a/b$ between the sides of the rectangle. Moreover, the corners of this hole never achieve an infinite curvature. Since the rectangular hole representing the artificial crack is always with rounded-off corners it can be studied analytically by mapping

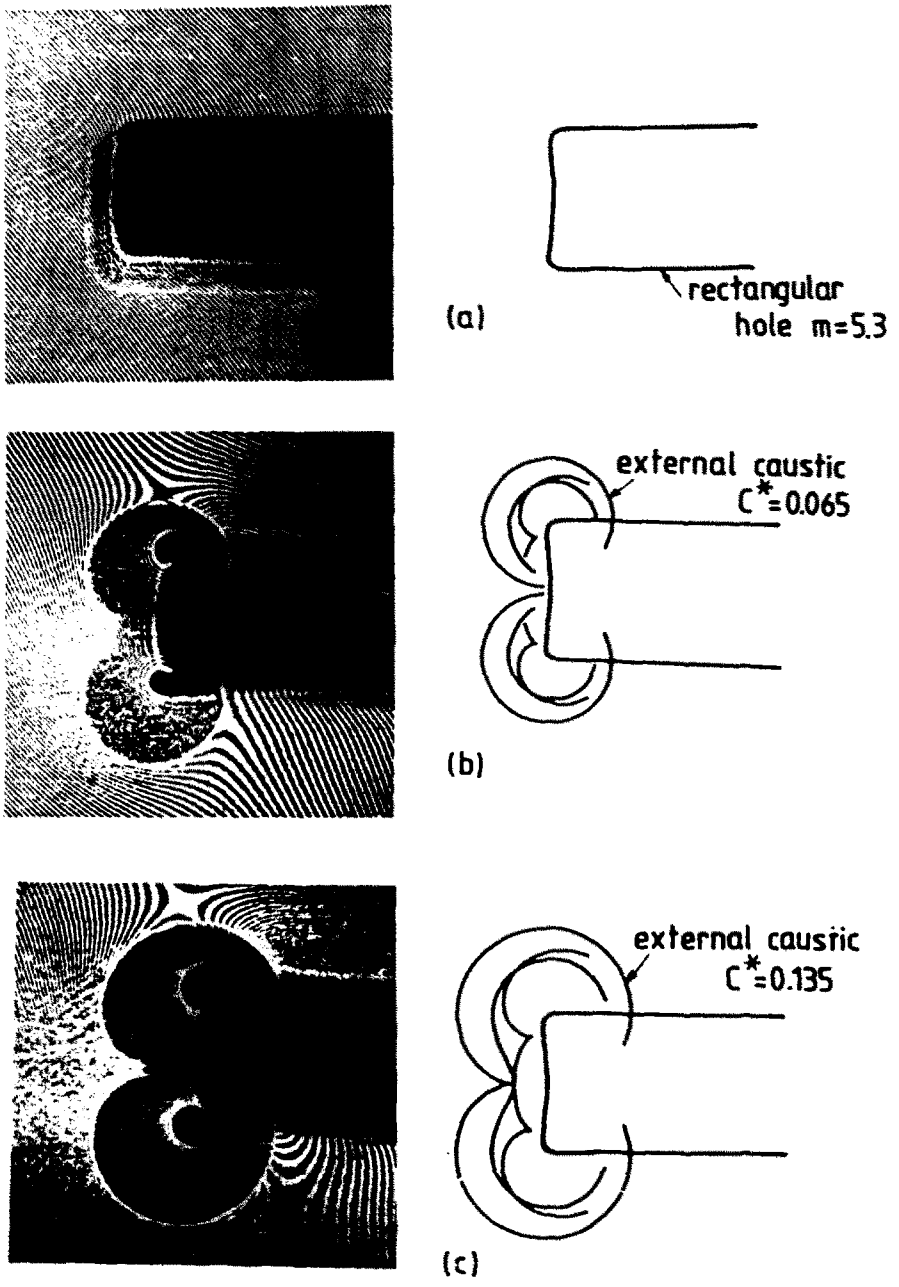

Fig. 8. The unloaded perforated plate for $m = 5.3$ (a) and the theoretical and experimental caustics for the loaded plate with $C^* = 0.065$ (b) and $C^* = 0.135$ (c).

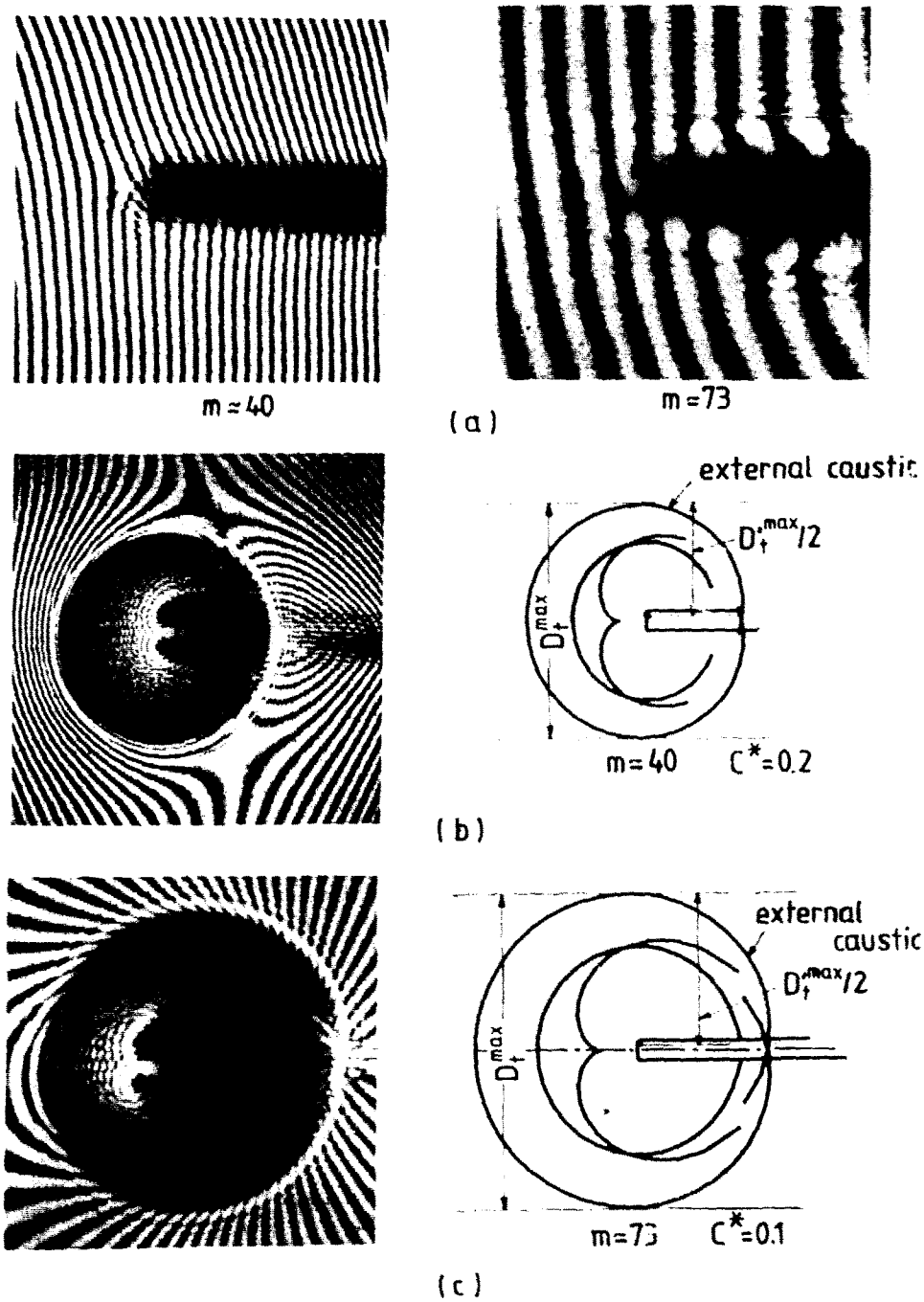

Fig. 9. The unloaded perforated plates for $m = 40$ and 73 in a magnification corresponding to $\lambda_m = 15.0$ (a). The experimental and theoretical caustics corresponding to C^* given by $C^* = 0.2$ for $m = 40$ (b) and $C^* = 0.1$ for $m = 73$ (c).

its shape inside the unit circle, using the Schwarz–Christoffel conformal mapping method, and defining the corresponding complex stress function $\varphi(\zeta)$ according to the theory of Muskhelishvili.

Comparing the tangential components of stress along the boundaries of the rectangular hole of Fig. 2, as well as the u_z-displacements along these boundaries, shown in Fig. 3, we make the following remarks.

(1) The singular points corresponding to either tip of the crack, which are unique for the natural cracks, are doubled.

(2) The whole boundary of the natural crack presents positive u_z-displacements except at the crack tips where each undeformed tip is split into two points one of which goes to minus infinity and represents the bottom of the crater formed around the crack tip, while the other is raised to the same height as the boundaries of the crack constituting the extremity of the ridge formed by the lips of the crack (see Fig. 2 in Theocaris and Petrou (1987)).

On the contrary, the minor sides of the artificial crack $C_1A_1A_2C_2$ in Fig. 2 are under negative u_z-displacements, whereas the major sides M_1C_1 and M_2C_2 are under positive u_z-displacements. Moreover, the unrealistic phenomenon of the double displacement of the crack tip, due to the influence of singularity there, disappears.

(3) Along the major axis of the artificial crack the u_z-gradients are negative along the B'_1S parts and positive along the remaining SL' parts of the axis, close to the tips of the crack. This variation of the gradients of u_z-displacements, which pass through zero values at points S close to the small sides, were detected by the rear-face caustics presenting cusps, when their respective initial curves lie inside the segment KS shown in Fig. 4(c).

(4) The method of reflected caustics was used in the present study to define the positions of the virtual singular points at the corners of the artificial crack, the values of SIFs and SOs, which define accurately the stress field in the cracked plate. The definition of these points was based on the obligation to have the initial curves and caustics to coincide with the caustics derived from the exact solution.

(5) The exact forms of the caustics shown in Fig. 4 separated the loading amplitude of the plate into three distinct zones. The first zone corresponds to cases of loading creating initial curves of a radius $r_0/b < 0.12$ having their centres at the apices of the corners. In this zone the measurement of the angular displacement of the caustic, and the ratio of the maximum diameter of the caustic and the radius r_0 of the initial curve (which for this zone is a single circle) allow the evaluation of the respective SIF and SO. It was found that for this zone the order of singularity tends to the value $\lambda = 0.455$.

(6) The second zone is defined by the circles contained in the interval $0.12 < r_0/b \leqslant 1.20$. In this zone the initial have also their centre at the apices of the corners of the crack. However, the two regions around each corner influence each other and the angular displacements of the caustics are large not corresponding to the orders of singularity defined by the ratios of the maximum diameters of the caustics and the respective radii of the initial curves.

This intermediate zone, therefore, may be characterized as an unstable one for the caustics yielding curves represented in Fig. 4(a) and (b).

(7) In the exterior zone, extending outside $r_0 = 1.2b$, the respective caustics attain a stable status, corresponding to the forms derived from natural cracks (see Fig. 4(c)).

(8) By examining the initial curve in the third zone we may observe that this curve is not a unique circle but it consists of two circular parts the centres of which appear in Fig. 4.

(9) If the stress field around the artificial crack is to be described only by the singular term the positions of the centres of these circular parts of the initial curve, which lie inside the rectangular hole, should be used as the origins of the coordinates for tracing the initial curves and the caustics.

(10) The values of the stress singularities λ and of the SIFs, normalized to the applied stress p at infinity, are contained in Tables 2–4 for rectangular holes with $m = 39.8$, 72.9 and ∞. The variation of the radii of the initial curves, normalized to the half crack length a, are presented in Fig. 7 vs the overall constant, C^*.

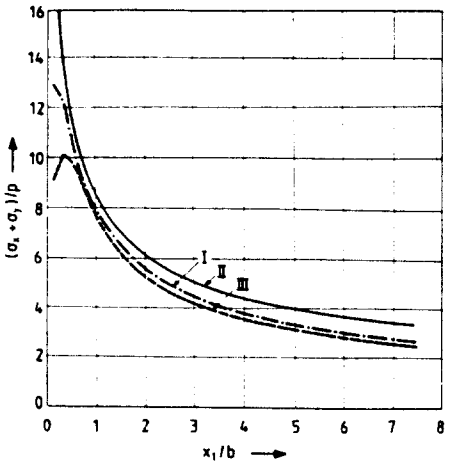

Fig. 10. The $(\sigma_x+\sigma_y)$-sum stresses, normalized to the external stress p, vs the x_1/a coordinate of the points of the first curve (Fig. 8). By (I) it is indicated the theoretical values, by (II) the values of the sum corresponding to $K_1/p = \sqrt{(a/2)} = 0.603m^{-1/2}$ and $\lambda = 0.5$ and by (III) the values of sum corresponding to $K_1/p = 0.4208m^{-1.43}$ and $\lambda = 0.57$ (see Table 3). The centres k_1 of the respective initial curves had coordinates $x_{0k}/b = 36.35$ and $y_{0k}/b = 0.25$, respectively.

(11) It is possible from information taken from this curve to select the appropriate experimental quantities for a given material and a given thickness of the plate and applied load to the specimen so that for a given rectangular crack with defined dimensions to obtain an accurate measurement in the desired neighbourhood of the crack by using only the singular term of the solution.

(12) It is clear from the graphs already presented that the radii of the initial curves for the natural crack and the respective artificial crack are not equal for the cases when $m \ll \infty$ apart from a very small region around the crack tip and only for values of the constant C^* lying in the interval $0 < C^* \leqslant 0.02$. However, also in this region the values of the order of singularities differ between them.

Up to now the method of caustics was also applied to artificial cracks with side ratios lying in the interval $40 \leqslant m \leqslant 80$ and the respective SIFs were evaluated based on the singular solution. The values of C^* given in the experiments were such that the error did not exceed 5% (see columns 13 in Tables 2–4). Thus, the value of SIF for the natural crack was defined by this procedure by assuming the order of singularity equal to $\lambda = 1/2$.

The values of the sum of the normal stresses along the longitudinal axis of the rectangular hole were plotted in Fig. 10 from the exact solution (curve I), the singular one (curve II), and the solution derived by applying the method of the paper, which takes into account the virtual centre of the initial curve as the origin of coordinates and the virtual value of the order of singularity for determining the SIF from the respective caustic (curve III). It is clear from these graphs that the values of the $(\sigma_x+\sigma_y)$-sum of stresses presented in curve III are very close to the exact solution (curve I) much better than the discrepancies between curves I and II.

The experimentally obtained caustics shown in Fig. 8 corroborate the results derived from the theoretical considerations. Figure 8(b) and (c) present caustics corresponding to the second zone where $r_0 \leqslant 1.2b$.

Figure 9 presents the caustics corresponding to the third zone for $m \simeq 40$ and 73 and $C^* = 0.2$ and 0.1, respectively. In these cases the diameter of the caustic D_t^{max}, represented in Fig. 4(c), defines the value of the K_1-factor, based on the singular solution, with an accuracy equal to $\pm 1\%$. However, if we evaluate the SIF with the virtual values of the stress singularity given in Tables 2 and 3, respectively, and determining the $D_t'^{max}$ from Fig. 7, the value of the SIF presents the same accuracy with the previously stated value.

As a final conclusion it may be stated that the use of artificial cracks in experiments for the study of natural cracks presents several and important discrepancies concerning the stress and strain fields of the cracked plate for high levels of loading of the plate. Particularly

dangerous is the use of artificial cracks in problems of dynamic fracture, where the artificial crack always engenders crack kinks from the corners of the rectangle always avoiding a crack nucleation along the artificial crack axis.

However, by using the method developed in this paper it is possible to circumvent many of these difficulties and obtain a clear and correct picture of the stress field in the cracked plate by using only a singular solution were the position of the stress singularity and its order are exactly defined from the shape of the artificial crack and the characteristics of the loading mode and the experimental arrangement of the experiment.

REFERENCES

Greager, M. and Paris, P. C. (1967). Elastic field equations for blunt cracks with reference to stress corrosion cracking. *Int. J. Fracture* **3**, 247–252.

Muskhelishvili, N. I. (1953). *Some Basic Problems of Mathematical Theory of Elasticity*, 3rd Edn, Chap. 21. Noordhoff, Groningen, The Netherlands.

Savin, G. N. (1961). *Concentration Around Holes* (Translated from Russian by W. Johnson), Chap. II, pp. 41–69. Pergamon Press, Oxford.

Smirnov, V. I. (1933). *Course in Higher Mathematics*, Vol. III. Costekhteoretizdat, Moscow.

Theocaris, P. S. (1986a). The internal crack in an extended or compressed plate: its geometric characteristics. *Engng Fract. Mech.* **26**, 753–770.

Theocaris, P. S. (1974). The order of singularity at a multi-wedge corner of composite plate. *Int. J. Engng Sci.* **12**, 107–120.

Theocaris, P. S. (1986b). Yield criteria based on void coalescence mechanisms. *Int. J. Solids Structures* **22**, 445–466.

Theocaris, P. S. (1981). Elastic stress intensity factors evaluated by caustics. In *Experimental Determination of Crack Tip Stress Intensity Factors, Mechanics of Fracture* (Edited by G. C. Sih), Vol. VII, Chap. 3, p. 189. Nijhoff, The Hague.

Theocaris, P. S. (1975). Stress and displacement singularities near corners. *J. Appl. Mech. Phys.* **26**, 77–98.

Theocaris, P. S. and Pazis, D. (1983). The topography of the core region around cracks under mode I, II, III of fracture. *Int. J. Mech. Sci.* **25**, 121–136.

Theocaris, P. S. and Petrou, L. (1986). Stress distributions and intensities at corners of equilateral triangular hole. *Int. J. Fracture* **31**, 271–289.

Theocaris, P. S. and Petrou, L. (1987). On the equivalent order of crack tip singularity defined by caustics. *Int. J. Fracture* **35**(4), 269–282.

Theocaris, P. S. and Prassianakis, J. (1980). Stress intensity factors in elastic plates with re-entrant corners asymmetrically loaded. *J. Strain Analysis* **15**(4), 195–200.

Zhen-Bang Kuang (1982). The stress field near the blunt crack tip and the fracture criterion. *Int. J. Engng Fract. Mech.* **16**, 19–23.

Williams, M. L. (1957). On the stress distribution at the base of stationary crack. *J. Appl. Mech.* **24**, 109–114.